Magnetism and Superconductivity in the t–J Model of $La_3Ni_2O_7$ Under Multiband Gutzwiller Approximation

Jie-Ran Xue(薛洁然)[1] and Fa Wang(王垡)[1,2*]

[1]*International Center for Quantum Materials, School of Physics, Peking University, Beijing 100871, China*
[2]*Collaborative Innovation Center of Quantum Matter, Beijing 100871, China*

(Received 22 February 2024; accepted manuscript online 16 April 2024)

The recent discovery of possible high temperature superconductivity in single crystals of $La_3Ni_2O_7$ under pressure renews the interest in research on nickelates. The density functional theory calculations reveal that both d_{z^2} and $d_{x^2-y^2}$ orbitals are active, which suggests a minimal two-orbital model to capture the low-energy physics of this system. In this work, we study a bilayer two-orbital t–J model within multiband Gutzwiller approximation, and discuss the magnetism as well as the superconductivity over a wide range of the hole doping. Owing to the inter-orbital super-exchange process between d_{z^2} and $d_{x^2-y^2}$ orbitals, the induced ferromagnetic coupling within layers competes with the conventional antiferromagnetic coupling, and leads to complicated hole doping dependence for the magnetic properties in the system. With increasing hole doping, the system transfers to A-type antiferromagnetic state from the starting G-type antiferromagnetic (G-AFM) state. We also find the inter-layer superconducting pairing of $d_{x^2-y^2}$ orbitals dominates due to the large hopping parameter of d_{z^2} along the vertical inter-layer bonds and significant Hund's coupling between d_{z^2} and $d_{x^2-y^2}$ orbitals. Meanwhile, the G-AFM state and superconductivity state can coexist in the low hole doping regime. To take account of the pressure, we also analyze the impacts of inter-layer hopping amplitude on the system properties.

DOI: 10.1088/0256-307X/41/5/057403

Since the discovery of high-T_c superconductivity in cuprates, extensive experimental and theoretical efforts have been made to explain the pairing mechanism in these compounds. Most of the theoretical studies suggested that the d^9 electronic configuration of Cu^{2+} and quasi-two-dimensional CuO_2 layers play critical roles in cuprate superconductivity. Considering that Ni^+ is isoelectronic with Cu^{2+}, the search for unconventional superconductivity in nickelates has become one major focus in condensed matter community.[1–11] Although superconductivity has been discovered in several nickelates, such as hole-doped infinite-layer nickelates $Nd_{1-x}Sr_xNiO_2$, the maximum of transition temperature T_c is just over 30 K and superconductivity only appears in thin films. Recently, evidences of superconductivity were observed in single crystal $La_3Ni_2O_7$ under pressure, and the transition temperature T_c can reach 80 K.[12] This experimental discovery immediately attracts great attention, and provides a new platform for researches of high-T_c superconductivity.

According to the Zhang–Rice singlets picture,[13] the low-energy physics of cuprates can be well described by a one-band Hubbard model, while situation becomes more complex in nickelates. The average valence of Ni in $La_3Ni_2O_7$ is $d^{8-\delta}$ with $\delta = 0.5$ for the superconducting samples, and density functional theory (DFT) calculations reveal that both the d_{z^2} orbital and $d_{x^2-y^2}$ orbital contribute to the bands near the Fermi level.[12,14–16] Owing to the apical oxygen between Ni–O bilayers, the d_{z^2} orbitals has strong inter-layer hopping and can form bonding-antibonding molecular-orbital states, results in energy splitting between d_{z^2} and $d_{x^2-y^2}$ orbitals. The above composite scenario suggests a two-orbital minimal model, where d_{z^2} is half-filled and $d_{x^2-y^2}$ is quarter-filled. We believe that two electrons at the same site prefer to form high-spin ($S = 1$) configuration, since Hund's coupling, denoted as J_H hereafter, is much larger than the splitting energy between d_{z^2} and $d_{x^2-y^2}$ orbitals.[17–19] In the large J_H limit, we also include the intra-orbital and inter-orbital Hubbard interactions, and derive an effective bilayer t–J model to describe the low-energy physics of $La_3Ni_2O_7$. A similar model has been used to study the superconducting nickelate $Nd_{1-x}Sr_xNiO_2$.[20]

There are already many theoretical[14,15,17,19,21–50] and experimental studies[51–60] for the bilayer nickelate $La_3Ni_2O_7$. Most of these works focus on the pairing mechanism and pairing symmetry in the superconducting phase. Some studies emphasize the similarity of the electronic structures between nickelates and cuprates, and further suggest that the strong hybridization between O $2p$ orbitals and Ni $3d$ orbitals will lead to the emergence of Zhang–Rice singlets and d-wave pairing in nickelates.[43] Other works believe that the d_{z^2} orbitals play an important role in these nickelates. Within this class of works, some researchers believe that the enhancement of the inter-layer hopping of d_{z^2} orbitals under pressure can induce the metallization of the energy band originating from d_{z^2} orbitals,[12,42] which is beneficial to superconductivity. Some other researchers have further studied the interaction between d_{z^2} and $d_{x^2-y^2}$ orbitals, and derived various multiband models for these materials. Some of these mod-

*Corresponding author. Email: wangfa@pku.edu.cn
© 2024 Chinese Physical Society and IOP Publishing Ltd

els are predicted to produce $s_{\pm}$ pairing symmetry.[15,31–37] There are also a few theoretical works about possible magnetism in $La_3Ni_2O_7$.[46–48] However, the interplay between magnetism and superconductivity, which is an extremely important issue in Cu- and Fe-based high-T_c superconductivity, has not been carefully studied in the context of $La_3Ni_2O_7$.

In this Letter, we study a bilayer t–J model for $La_3Ni_2O_7$ using multiband Gutzwiller approximation, to have a comprehensive understanding of the ground state properties of this system at different band filling. We find that inter-layer s-wave superconducting pairing of $d_{x^2-y^2}$ orbitals dominates and coexists with G-type antiferromagnetic (G-AFM) order in the low doping region. Meanwhile, superconductivity can be enhanced with increasing inter-layer hopping amplitude. With increasing hole doping, the system transfers to A-type antiferromagnetic (A-AFM) state. In the following, we first introduce the minimal two-orbital model and the derived bilayer t–J Hamiltonian. Then, we describe the procedures of performing the multiband Gutzwiller approximations and determining the renormalized mean-field Hamiltonian in detail. We present the numerical results obtained by solving the renormalized mean-field Hamiltonian in a self-consistent manner, and discuss the interplay of superconductivity, antiferromagnetism, as well as ferromagnetism in a wide range of hole doping. Finally, we present our conclusions and comparison with previous studies.

Bilayer t–J Model and Effective Mean-Field Hamiltonian. We start from a two-orbital (Ni−d_{z^2} and Ni−$d_{x^2-y^2}$) model on a bilayer square lattice [as depicted in Fig. 1(a)]:

$$\begin{aligned} H &= H_t + \frac{U_1}{2}\sum_{il} n_{1l;i}(n_{1l;i}-1) + \frac{U_2}{2}\sum_{il} n_{2l;i}(n_{2l;i}-1) \\ &\quad + U'\sum_{il} n_{1l;i}n_{2l;i} - 2J_{\rm H}\sum_{il}(\boldsymbol{S}_{1l;i}\cdot\boldsymbol{S}_{2l;i} + \frac{1}{4}n_{1l;i}n_{2l;i}), \\ H_t &= \sum_{il\alpha}\epsilon_\alpha n_{\alpha l;i} + \sum_{\langle ij\rangle}\sum_{l\sigma\alpha\beta} t^{\rm intra}_{\alpha\beta} c^\dagger_{\alpha l;i\sigma}c_{\beta l;j\sigma} \\ &\quad + \sum_{il\sigma\alpha\beta} t^{\rm inter}_{\alpha\beta} c^\dagger_{\alpha l;i\sigma}c_{\beta\bar{l};i\sigma}, \end{aligned} \tag{1}$$

where $l = t, b$ labels the top and bottom layers, $\alpha/\beta = 1, 2$ denotes the two orbitals d_{z^2} and $d_{x^2-y^2}$, respectively, and $\sigma =\uparrow, \downarrow$ labels the spin; $\langle ij\rangle$ denotes the nearest neighbor within each layer; $n_{\alpha l;i} = \sum_\sigma c^\dagger_{\alpha l;i\sigma}c_{\alpha l;i\sigma}$ is the particle number operator of orbital α at site i within layer l, and $\boldsymbol{S}_{\alpha l;i} = \frac{1}{2}\sum_{\sigma\sigma'} c^\dagger_{\alpha l;i\sigma}\boldsymbol{\sigma}_{\sigma\sigma'}c_{\alpha l;i\sigma'}$ is the spin operator. We consider the onsite intra-orbital Hubbard interaction U_1 and U_2, inter-orbital repulsion U' and Hund's coupling $J_{\rm H}$. We assume $U_1 = U_2 = U$ and adopt Kanamori relation $U = U' + 2J_{\rm H}$.[61] Here ϵ_α is the onsite energy and reflects the splitting energy between the two orbitals. According to the DFT calculation,[14] we take $t^{\rm intra}_{11} = -0.11$, $t^{\rm intra}_{22} = -0.483$, $t^{\rm intra}_{12} = 0.239$, $t^{\rm inter}_{22} = 0.005$, $t^{\rm inter}_{12} = 0$, $\epsilon_0 = 0$ and $\epsilon_1 = 0.367$. Meanwhile, we set $U = 4$, $U' = 2$, and $J_{\rm H} = 1$.[17–19,48] We use electron volt (eV) as the energy unit throughout this study. With varying pressure, the inter-layer hopping amplitude for orbital d_{z^2} may significantly increase,[35] and our work considers different values of $t^{\rm inter}_{11}(= -0.5, -0.6, -0.7)$. In addition, the average valence of Ni is $d^{8-\delta}$, where δ is the hole doping.

In the large $J_{\rm H}$ limit, we project to the restricted Hilbert space, which consists five states at each site.[20] We suppress the site and layer labels for brevity here. We label two singlon states with $|\sigma\rangle = c^\dagger_{1;\sigma}|0\rangle$, $\sigma =\uparrow, \downarrow$, and three doublon states with $|x\rangle = -\frac{1}{\sqrt{2}}(c^\dagger_{1;\uparrow}c^\dagger_{2;\uparrow} - c^\dagger_{1;\downarrow}c^\dagger_{2;\downarrow})|0\rangle$, $|y\rangle = \frac{i}{\sqrt{2}}(c^\dagger_{1;\uparrow}c^\dagger_{2;\uparrow} + c^\dagger_{1;\downarrow}c^\dagger_{2;\downarrow})|0\rangle$, and $|z\rangle = \frac{1}{\sqrt{2}}(c^\dagger_{1;\uparrow}c^\dagger_{2;\downarrow} + c^\dagger_{1;\downarrow}c^\dagger_{2;\uparrow})|0\rangle$. The spin operator $\boldsymbol{S}^{\rm s}$ for spin-1/2 singlon and spin operator $\boldsymbol{S}^{\rm d}$ for spin-1 doublon can be written as $(\boldsymbol{S}^{\rm s})^a = \frac{1}{2}\sum_{\sigma\sigma'}(\sigma_a)_{\sigma\sigma'}|\sigma\rangle\langle\sigma'|$ and $(\boldsymbol{S}^{\rm d})^a = -i\sum_{bc}\epsilon_{abc}|b\rangle\langle c|$ with Pauli matrix σ and antisymmetric tensor ϵ.

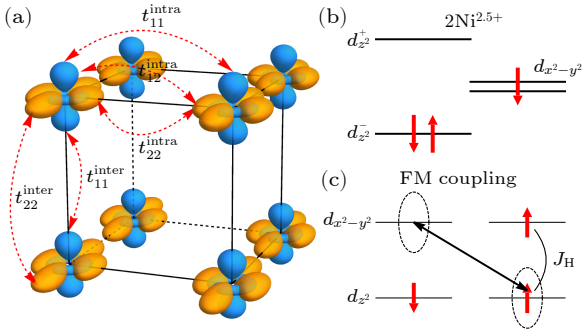

Fig. 1. (a) Schematic of the bilayer two-orbital model with hopping parameters in the Hamiltonian. (b) Electronic configuration in two atoms with the same planar site, where $d^+_{z^2}$ represents the anti-bonding state and $d^-_{z^2}$ is the bonding states. (c) The inter-orbital superexchange process which induces the ferromagnetic coupling.

We treat the kinetic terms as perturbations and perform the standard second-order perturbation theory, reaching the bilayer t–J model:

$$\begin{aligned} H_{t-J} &= \sum_{\langle ij\rangle l\sigma} t^{\rm intra}_{22} c^\dagger_{2l;i\sigma}c_{2l;j\sigma} + \sum_{il\sigma} t^{\rm inter}_{22} c^\dagger_{2l;i\sigma}c_{2\bar{l};i\sigma} + H_J, \\ H_J &= J_1\sum_{\langle ij\rangle l}(\boldsymbol{S}^{\rm s}_{l;i}\cdot\boldsymbol{S}^{\rm s}_{l;j} - \frac{1}{4}n^{\rm s}_{l;i}n^{\rm s}_{l;j}) \\ &\quad + J_2\sum_i(\boldsymbol{S}^{\rm s}_{1;i}\cdot\boldsymbol{S}^{\rm s}_{2;i} - \frac{1}{4}n^{\rm s}_{1;i}n^{\rm s}_{2;i}) \\ &\quad + J_{d1}\sum_{\langle ij\rangle l}(\boldsymbol{S}^{\rm d}_{l;i}\cdot\boldsymbol{S}^{\rm d}_{l;j} - n^{\rm d}_{l;i}n^{\rm d}_{l;j}) \\ &\quad + J_{d2}\sum_i(\boldsymbol{S}^{\rm d}_{1;i}\cdot\boldsymbol{S}^{\rm d}_{2;i} - n^{\rm d}_{1;i}n^{\rm d}_{2;i}) \\ &\quad + \frac{1}{2}J'_1\sum_{\langle ij\rangle l}[(\boldsymbol{S}^{\rm s}_{l;i}\cdot\boldsymbol{S}^{\rm d}_{l;j} - \frac{1}{2}n^{\rm s}_{l;i}n^{\rm d}_{l;j}) + (s\leftrightarrow d)] \\ &\quad + \frac{1}{2}J'_2\sum_i[(\boldsymbol{S}^{\rm s}_{1;i}\cdot\boldsymbol{S}^{\rm d}_{2;i} - \frac{1}{2}n^{\rm s}_{1;i}n^{\rm d}_{2;i}) + (s\leftrightarrow d)], \end{aligned} \tag{2}$$

where J_1 (J_2) is the antiferromagnetic spin coupling within (between) layers, J_{d1} (J_{d2}) is the spin coupling between doublons, and J'_1 (J'_2) can be viewed as Kondo coupling between singlon and doublon. More details of these parameters are shown in the Supplementary Material. In Table 1, we show the resulting spin coupling parameters with the tight-binding parameters listed above. Here $n^{\rm s}_{l;i}$

and $n^{\rm d}_{l;i}$ are the density operators of singlon and doublon.

Table 1. The spin coupling parameters for the derived effective bilayer t–J model with different values of inter-layer hopping amplitude $t_{11}^{\rm inter}$.

$t_{11}^{\rm inter}$	J_1	J_1'	J_{d1}	J_2	J_2'	J_{d2}
0.5	0.046	0.029	0.072	0.25	0.125	0.05
0.6	0.046	0.029	0.072	0.36	0.18	0.072
0.7	0.046	0.029	0.072	0.49	0.245	0.098

We study the above t–J Hamiltonian using the Gutzwiller approximation,[62,63] and the trial wavefunction has the form:

$$|\psi\rangle = \frac{\hat{P}|\psi_0\rangle}{\langle\psi_0|\hat{P}^2|\psi_0\rangle}, \tag{3}$$

where $\hat{P}$ is the Gutzwiller projection operator assumed as

$$\begin{aligned}\hat{P} &= \prod_{il}\hat{P}(il),\\ \hat{P}(il) &= \sum_{\sigma}\eta_{1\sigma}(il)\hat{Q}_{1e,\sigma}(il)+\sum_{\sigma\sigma'}\eta_{2\sigma\sigma'}(il)\hat{Q}_{2e,\sigma\sigma'}(il).\end{aligned} \tag{4}$$

Here $\hat{Q}_{1e,\,\sigma}(il)$ is the projection operator to a singly occupied state of electron with spin σ from orbital 1 at site i and layer l, and $\hat{Q}_{2e,\,\sigma\sigma'}$ is the projection operator to a doublon state consisting of one spin σ electron from orbital 1 and one spin σ' electron from orbital 2 at site i and layer l; $\eta_{1\sigma}$ and $\eta_{2\sigma\sigma'}$ are fugacities which control the relative weight of states and ensure the local densities are same before and after the projection, that is, $\langle n_{\alpha l;i\sigma}\rangle = \langle n_{\alpha l;i\sigma}\rangle_0$. These parameters are determined self-consistently in this work, and the explicit expressions are shown in the Supplementary Material.

In order to search for the minimum of energy $E = \langle\psi|H_{t-J}|\psi\rangle$, we first define the following expectation values: the average number $n_{\alpha l;i\sigma} = \langle\psi_0|c^\dagger_{\alpha l;i\sigma}c_{\alpha l;i\sigma}|\psi_0\rangle$, hopping amplitudes $\chi^{\rm intra}_{(\alpha l;i\sigma)(\beta l;j\sigma)} = \langle\psi_0|c^\dagger_{\alpha l;i\sigma}c_{\beta l;j\sigma}|\psi_0\rangle$ and $\chi^{\rm inter}_{(\alpha l;i\sigma)(\alpha\bar{l};i\sigma)} = \langle\psi_0|c^\dagger_{\alpha l;i\sigma}c_{\alpha\bar{l};i\sigma}|\psi_0\rangle$, and pairing order parameter $\Delta^{\rm intra}_{(\alpha l;i\sigma)(\alpha l;j\bar{\sigma})} = \langle\psi_0|c_{\alpha l;i\sigma}c_{\alpha l;j\bar{\sigma}}|\psi_0\rangle$ and $\Delta^{\rm inter}_{(\alpha l;i\sigma)(\alpha\bar{l};i\bar{\sigma})} = \langle\psi_0|c_{\alpha l;i\sigma}c_{\alpha\bar{l};i\bar{\sigma}}|\psi_0\rangle$. We only consider the intra-orbital spin-singlet pairing and neglect the inter-orbital hopping term between layers. Site i and site j are the nearest neighbors. By applying Wick's theorem, the energy E is a function of these expectation values, and the solution of $|\psi_0\rangle$ amounts to the ground state of the following effective mean-field Hamiltonian:

$$\begin{aligned}H_{\rm eff} = &\sum_{\langle ij\rangle l\alpha\beta\sigma} g^t_{(\alpha l;i\sigma)(\beta l;j\sigma)}c^\dagger_{\alpha l;i\sigma}c_{\beta l;j\sigma}\\ &+\sum_{il\alpha\sigma} g^t_{il\alpha\sigma}c^\dagger_{\alpha l;i\sigma}c_{\alpha\bar{l};i\sigma}\\ &+\sum_{il\alpha\sigma}\Big(\frac{1}{2}\sigma h_{il\alpha}-\mu_\alpha\Big)c^\dagger_{\alpha l;i\sigma}c_{\alpha l;i\sigma}\\ &+\sum_{\langle ij\rangle l\alpha} g^I_{ijl\alpha}(c_{\alpha l;i\uparrow}c_{\alpha l;j\downarrow}-c_{\alpha l;i\downarrow}c_{\alpha l;j\uparrow})+\text{h.c.}\\ &+\sum_{i\alpha} g^I_{i\alpha}(c_{\alpha 1;i\uparrow}c_{\alpha 2;i\downarrow}-c_{\alpha 1;i\downarrow}c_{\alpha 2;i\uparrow})+\text{h.c.},\end{aligned} \tag{5}$$

where the expressions for the parameters are given by

$$\begin{aligned}g^t_{(\alpha l;i\sigma)(\beta l;j\sigma)} &= \frac{\partial E}{\partial\chi^{\rm intra}_{(\alpha l;i\sigma)(\beta l;j\sigma)}},\\ g^t_{il\alpha\sigma} &= \frac{\partial E}{\partial\chi^{\rm inter}_{(\alpha l;i\sigma)(\alpha\bar{l};i\sigma)}},\\ h_{il\alpha} &= \frac{\partial E}{\partial n_{\alpha l;i\uparrow}}-\frac{\partial E}{\partial n_{\alpha l;i\downarrow}},\\ g^I_{ijl\alpha} &= \frac{\partial E}{\partial\Delta^{\rm intra}_{(\alpha l;i\uparrow)(\alpha l;j\downarrow)}},\\ g^I_{i\alpha} &= \frac{\partial E}{\partial\Delta^{\rm inter}_{(\alpha 1;i\uparrow)(\alpha 2;i\downarrow)}},\end{aligned} \tag{6}$$

we adopt a self-consistent process to solve this mean-field Hamiltonian and obtain the solution of $|\psi_0\rangle$. We present our numerical results in the following.

The Numerical Result of the Bilayer t–J Model. The super-exchange couplings within layers are several times smaller than those between layers due to the large hopping parameter $t_{11}^{\rm inter}$. The strong coupling of orbital d_{z^2} between layers can be shared to orbital $d_{x^2-y^2}$ with large Hund's coupling, and induces finite inter-layer s-wave pairing of orbital $d_{x^2-y^2}$ in spite of small hopping for $d_{x^2-y^2}$ between layers. This kind of pairing effectively suppresses intra-layer cuprate-like d-wave pairing, which is similar to the bilayer Hubbard models studied previously[64,65] and can be verified by our numerical calculations. Meanwhile, second-order perturbation theory shows that the inter-orbital superexchange process between the half-filled and empty orbital can lead to ferromagnetic coupling,[46,66] as shown in Fig. 1(c). Thus, we analyze both A-AFM and G-AFM tendencies in the system and explore the possibility of the coexistence of superconductivity and magnetism.

The obtained magnetic order, superconducting order and energy as a function of hole doping are displayed in Fig. 2. In the low doping limit, the intra-layer ferromagnetic order is absent until hole doping $\delta \approx 0.10$ [see Fig. 2(a)], and this is consistent with the super-exchange picture we mentioned above, as small hole doping value leads to fewer empty orbitals. With increasing hole doping, the system tends to form the A-AFM state, the calculated magnetic order of $d_{x^2-y^2}$ decreases linearly with hole doping and the magnetic order of d_{z^2} remains at 0.5; while the G-AFM state has the largest magnetic order value at $\delta = 0$, where both orbitals are half-filled and the antiferromagnetic coupling determines the ground state of the system. The strong Hund's coupling aligns the spin of the two orbitals, and causes the G-AFM orders of the two orbitals decrease simultaneously, though the filling of d_{z^2} is fixed, and eventually vanish around $\delta = 0.56$. Upon increasing $t_{11}^{\rm inter}$, the magnetic properties of the system do not change much as displayed in Figs. 2(d) and 2(e).

Figure 2(b) demonstrates the doping dependence of the calculated superconducting order parameters with and without magnetic order. Within the Gutzwiller approximation we adopted, only the intra-orbital pairing of $d_{x^2-y^2}$ orbitals survives and the numerical calculations end up with s-wave spin-singlet pairing, different from the d-wave pairing in cuprate. The intra-layer pairing orders are much weaker compared to the inter-layer pairing order, since

the large inter-layer super-exchange coupling of d_{z^2} orbitals due to strong hopping along the vertical inter-layer bond can be shared to $d_{x^2-y^2}$ orbital. With G-AFM order, the doping dependence of the superconducting pairing order shows more complicated feature. In order to explore the reason for this phenomenon, we substitute the self-consistent results of coexisting G-AFM and superconductivity (labeled as G-AFM+SC) phase into Eq. (6), and remove the pairing terms in the effective mean-field Hamiltonian. We find that in the low doping region ($\delta < 0.24$), there is no "Fermi surface". The Fermi surface here is not the physical Fermi surface, but derived from the modified mean-field Hamiltonian. However, in the pure G-AFM states, there are Fermi surfaces satisfying Luttinger volume constraint. This is an indication that the low doping superconducting states are in the BEC limit. The "gap" gradually decreases with increasing doping and goes to zero around $\delta = 0.24$ [the arrows in Fig. 2(f) point out the position where the Fermi surface appears, and we also gives one specific Fermi surface in the reduced magnetic Brillouin zone with $t_{11}^{\text{inter}} = -0.5$ and $\delta = 0.30$]. Thus we attribute the different behaviors of superconducting pairing order parameters in different doping ranges to the change in the Fermi surfaces of this system. We also notice that the magnetic order on $d_{x^2-y^2}$ orbitals in G-AFM phase abruptly increases near $\delta = 0.08$ in Fig. 2(a), we believe this phenomenon is also caused by the change in Fermi surfaces. With increasing t_{11}^{inter}, the value of optimal doping and magnitude of superconducting pairing order increase, which may explain the observed superconductivity in $La_3Ni_2O_7$ under pressure and suggest that electron doping this system may further enhance the superconductivity.

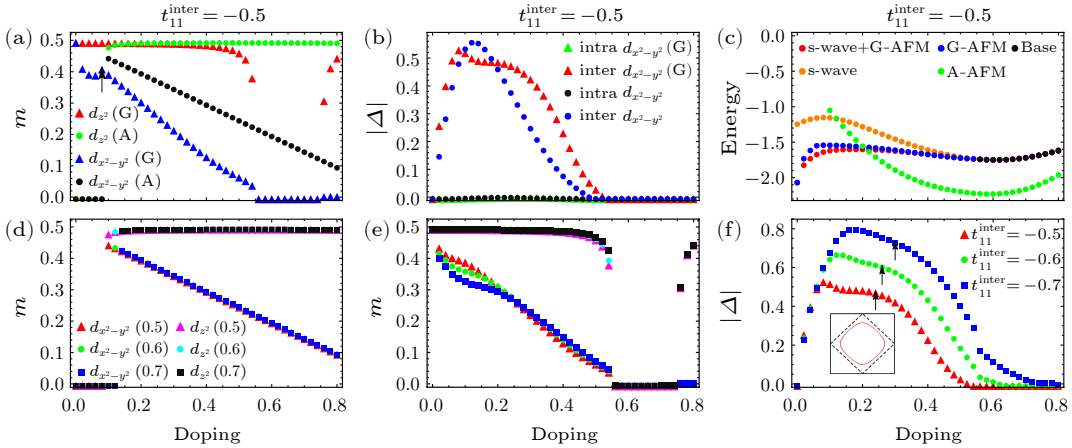

Fig. 2. The dependence of (a) magnetic order parameter, (b) pairing order parameter and (c) energy on hole doping δ for the bilayer t–J model with $t_{11}^{\text{inter}} = -0.5$. The variations of magnetic and pairing order parameters by tuning the inter-layer hopping amplitude t_{11}^{inter} are plotted in (d), (e), and (f). (a) The magnetic order parameters of both orbitals in G-AFM phase are maximized at $\delta = 0$ and gradually decrease with increasing doping; while the magnetic orders in A-AFM phase are absent in low-doping regime and appear near $\delta = 0.1$. (b) The intra-layer superconducting pairing order for both cases are negligible small, while the inter-layer pairing order in pure s-wave phase exhibits a dome shape and more complicated behaviors occur with a G-AFM background. In (c), we demonstrate the calculated energy for different states of the system. The black dots represent the states with neither magnetic order nor pairing order for comparison. We further analyze (d) the A-AFM states and [(e), (f)] G-AFM+SC states with different t_{11}^{inter}, find that the values of t_{11}^{inter} have less impacts on the magnetic properties of the systems, but the optimal doping as well as the magnitudes of pairing order are significant changed as displayed in (f).

As displayed in Fig. 2(c), the G-AFM+SC state has the lowest energy up to $\delta \approx 0.2$, but with a close energy for pure G-AFM state. Upon further increase of the hole doping, the system transfers to the A-AFM state.

As we mentioned above, the superconducting states with G-AFM order are in the BEC limit in low doping regimes, and the finite pairing order parameter is not enough to determine the onset of superconductivity. We therefore consider the superfluid stiffness, denoted as D_{s}, to distinguish different phases of the system. The superfluid stiffness reflects the diamagnetic Meissner effect of superconductors and is proportional to the superfluid density. Within Kubo formulism, the superfluid stiffness is determined by [67–69]

$$\frac{D_{\text{s}}}{\pi e^2} = \langle -k_x \rangle - \Lambda_{xx}(q_x = 0,\, q_y \to 0,\, \omega = 0), \tag{7}$$

where k_x is the kinetic energy along the x direction and represents the diamagnetic responds to an external vector potential A_x; while Λ_{xx} is the paramagnetic current-current correlation function, which can be obtained from

$$\Lambda_{xx}(\boldsymbol{q},\, i\omega_n) = \frac{1}{N}\int_0^\beta d\tau e^{i\omega_n \tau}\langle j_x^p(\boldsymbol{q},\, \tau) j_x^p(-\boldsymbol{q},\, 0)\rangle, \tag{8}$$

where $\omega_n = 2\pi nT$ (n is a positive integer) and the paramagnetic current $j_x^p(\boldsymbol{q})$ has the form:

$$j_x^p(\boldsymbol{q}) = \sum_{l\sigma\boldsymbol{k},\alpha\neq\beta} \frac{\partial t_{22}^{\text{intra}}(\boldsymbol{k}+\frac{\boldsymbol{q}}{2})}{\partial k_x} c_{2l;\alpha\sigma}^\dagger(\boldsymbol{k}+\boldsymbol{q}) c_{2l;\beta\sigma}(\boldsymbol{k}), \tag{9}$$

with $t_{22}^{\text{intra}}(\boldsymbol{k}) = 2t_{22}^{\text{intra}}(\cos(k_x/\sqrt{2}) + \cos(k_y/\sqrt{2}))$, $\alpha(\beta) = A/B$ labeling the sublattice since we are also interested in antiferromagnetic order in our work. Then we take

the analytic continuation $i\omega_n \to 0 + i\eta$, and use a function $A + Bq_y + Cq_y^2$ to fit data for small q_y in order to have an appropriate $q_y \to 0$ extrapolation. For simplicity, we approximately express the correlation function as $\Lambda_{xx} = g^2\Lambda^0_{xx}$, and the Gutzwiller renormalization factor g is defined as the ratio of the expectations of nearest-neighbor intra-orbital hopping of orbital $d_{x^2-y^2}$ after and before projection, that is, $g = \langle c^\dagger_{2l;i\sigma}c_{2l;j\sigma}\rangle / \langle c^\dagger_{2l;i\sigma}c_{2l;j\sigma}\rangle_0$. Meanwhile,

$$\Lambda^0_{xx}(\boldsymbol{q}, i\omega_n) = \frac{1}{N}\int_0^\beta \mathrm{d}\tau e^{i\omega_n\tau}\langle j^p_x(\boldsymbol{q}, \tau) j^p_x(-\boldsymbol{q}, 0)\rangle_0. \quad (10)$$

In Fig. 3(a), we plot the superfluid stiffness as a function of hole doping when the s-wave superconducting order and G-AFM order coexist. The superfluid stiffness at low doping is largely suppressed due to the reduction of the kinetic energy after projection as well as the Gutzwiller renormalization factor. Meanwhile, the superfluid stiffness is relatively small compared to the case without G-AFM background [Fig. 3(b)], since there is no Fermi surface around $\delta = 0$. Increasing hole doping, the superfluid stiffness keeps growing as the Fermi surface gradually forms. After reaching the maximum value, it begins to decrease and becomes basically zero, which is consistent with the result for metallic phase. In the superconducting region, the superfluid stiffness has larger optimal doping value compared to the magnitude of pairing order, and the value grows from 0.44 to 0.56 with increasing t_{11}^{inter} amplitude from 0.5 to 0.7.

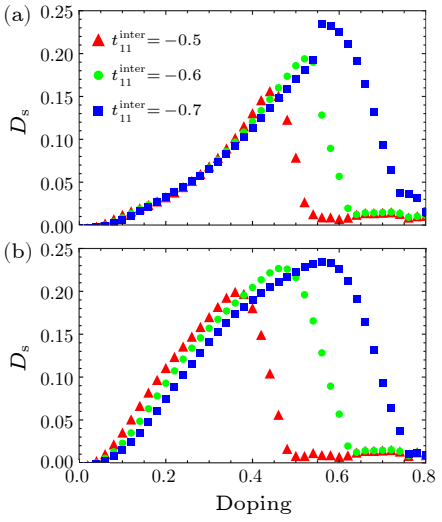

Fig. 3. The calculated superfluid stiffness as a function of hole doping with various t_{11}^{inter} in different phases. Superfluid stiffness (a) with and (b) without G-AFM background.

In summary, we have performed a detailed analysis of the effective bilayer t–J model using the multiband Gutzwiller approximation. Previous theoretical studies on this material using the Gutzwiller approximation mainly focused on the smaller values of J_{H},[32] and suggested large on-site intra-orbital pairing due to the pair-hopping interaction, while the intra-orbital pairing for d_{z^2} orbitals on the vertical bond is subleading. Here, we believe the nickelate $La_3Ni_2O_7$ is in the strong coupling regime and study the system in large J_{H} limit.[17–19] Meanwhile, we carefully incorporate more inter-site correlations and derive the relatively complicated renormalized mean-field Hamiltonian, which is considered to be a better choice to give satisfactory results for strong correlated materials.[63,70]

Our numerical results show that this model prefers to form s-wave superconducting pairing from $d_{x^2-y^2}$ orbitals due to strong inter-layer spin exchange interaction. The superconducting dome can extend over a wide doping range, including the doping value relevant for $La_3Ni_2O_7$, and the pairing order is enhanced with increasing inter-layer hopping t_{11}^{inter} of d_{z^2} orbitals [see Fig. 3(f)]. We notice the previous work by Wu *et al.* proposed the same scenario for superconductivity in $La_3Ni_2O_7$.[27] They also emphasized the significance of Hund's coupling and studied an effective bilayer single $d_{x^2-y^2}$-orbital model for $La_3Ni_2O_7$. Through the slave-boson approach, the authors of Ref. [27] found robust inter-layer s-wave pairing. Similar results were also obtained in the tensor-network analysis for this bilayer model.[28] In the low hole doping regime, we find that G-AFM state can coexist with superconductivity, similar to the result for a bilayer extended Hubbard–Heisenberg model,[71] and the absence of Fermi surface causes the low value of superfluid stiffness, which will greatly suppress the superconductivity. Unfortunately, the Gutzwiller approximation method we employ is not suitable for finite temperature calculations, therefore we could not produce a reliable estimate of the superconducting critical temperature for this G-AFM+SC phase.

Some previous DFT calculations[46] pointed out that $La_3Ni_2O_7$ may form magnetic ground state with strong electronic correlations. In our calculation, we find that the importance of intra-layer ferromagnetic couplings, produced by super-exchange processes between half-filled and empty orbitals, increases with increasing hole doping δ, so that the A-AFM state without coexisting superconductivity has the lowest energy for large doping value $\delta \gtrsim 0.2$.

Note Added. During the preparation of this article, we become aware of several works which study similar models.[39,40] However, we studied the interplay between magnetism and superconductivity which were not considered in those works.

Acknowledgement. This work was supported by the National Natural Science Foundation of China (Grant Nos. 12274004 and 11888101).

References

[1] Anisimov V I, Bukhvalov D, and Rice T M 1999 *Phys. Rev. B* **59** 7901
[2] Li D F, Lee K, Wang B Y, Osada M, Crossley S, Lee H R, Cui Y, Hikita Y, and Hwang H Y 2019 *Nature* **572** 624
[3] Osada M, Wang B Y, Goodge B H, Lee K, Yoon H, Sakuma K, Li D F, Miura M, Kourkoutis L F, and Hwang H Y 2020 *Nano Lett.* **20** 5735
[4] Zeng S W, Li C J, Chow L E, Cao Y, Zhang Z T, Tang C S, Yin X M, Lim Z S, Hu J X, Yang P, and Ariando A 2022 *Sci. Adv.* **8** eabl9927
[5] Li D F, Wang B Y, Lee K, Harvey S P, Osada M, Goodge B H, Kourkoutis L F, and Hwang H Y 2020 *Phys. Rev. Lett.* **125** 027001

[6] Osada M, Wang B Y, Lee K, Li D F, and Hwang H Y 2020 *Phys. Rev. Mater.* **4** 121801
[7] Zeng S W, Yin X M, Li C J, Chow L E, Tang C S, Han K, Huang Z, Cao Y, Wan D Y, Zhang Z T, Lim Z S, Diao C Z, Yang P, Wee A T S, Pennycook S J, and Ariando A 2022 *Nat. Commun.* **13** 743
[8] Yang C, Ortiz R A, Wang Y, Sigle W, Wang H G, Benckiser E, Keimer B, and van Aken P A 2023 *Nano Lett.* **23** 3291
[9] Wang N N, Yang M W, Yang Z, Chen K Y, Zhang H, Zhang Q H, Zhu Z H, Uwatoko Y, Gu L, Dong X L, Sun J P, Jin K J, and Cheng J G 2022 *Nat. Commun.* **13** 4367
[10] Gu Q Q and Wen H H 2022 *Innovation* **3** 100202
[11] Pan G A, Ferenc Segedin D, LaBollita H, Song Q, Nica E M, Goodge B H, Pierce A T, Doyle S, Novakov S, Córdova Carrizales D, N'Diaye A T, Shafer P, Paik H, Heron J T, Mason J A, Yacoby A, Kourkoutis L F, Erten O, Brooks C M, Botana A S, and Mundy J A 2022 *Nat. Mater.* **21** 160
[12] Sun H L, Huo M W, Hu X W, Li J Y, Liu Z J, Han Y F, Tang L Y, Mao Z Q, Yang P T, Wang B S, Cheng J G, Yao D X, Zhang G M, and Wang M 2023 *Nature* **621** 493
[13] Zhang F C and Rice T M 1988 *Phys. Rev. B* **37** 3759
[14] Luo Z H, Hu X W, Wang M, Wú W, and Yao D X 2023 *Phys. Rev. Lett.* **131** 126001
[15] Gu Y H, Le C, Yang Z S, Wu X X, and Hu J P 2023 arXiv:2306.07275 [cond-mat.supr-con]
[16] Pardo V and Pickett W E 2011 *Phys. Rev. B* **83** 245128
[17] Christiansson V, Petocchi F, and Werner P 2023 *Phys. Rev. Lett.* **131** 206501
[18] Cao Y Y and Yang Y F 2024 *Phys. Rev. B* **109** L081105
[19] Kumar U, Melnick C, and Kotliar G 2023 arXiv:2310.00983 [cond-mat.str-el]
[20] Zhang Y H and Vishwanath A 2020 *Phys. Rev. Res.* **2** 023112
[21] Wú W, Luo Z H, Yao D X, and Wang M 2024 *Sci. China Phys. Mech. Astron.* **67** 117402
[22] Yang Y F, Zhang G M, and Zhang F C 2023 *Phys. Rev. B* **108** L201108
[23] Lu D C, Li M, Zeng Z Y, Hou W, Wang J, Yang F, and You Y Z 2023 arXiv:2308.11195 [cond-mat.str-el]
[24] Schlömer H, Schollwöck U, Grusdt F, and Bohrdt A 2023 arXiv:2311.03349 [cond-mat.str-el]
[25] Chen J L, Yang F, and Li W 2023 arXiv:2311.05491 [cond-mat.str-el]
[26] Qu X Z, Qu D W, Li W, and Su G 2023 arXiv:2311.12769 [cond-mat.str-el]
[27] Lu C, Pan Z M, Yang F, and Wu C J 2024 *Phys. Rev. Lett.* **132** 146002
[28] Qu X Z, Qu D W, Chen J L, Wu C J, Yang F, Li W, and Su G 2024 *Phys. Rev. Lett.* **132** 036502
[29] Zheng Y Y and Wú W 2023 arXiv:2312.03605 [cond-mat.str-el]
[30] Lu C, Pan Z M, Yang F, and Wu C J 2023 arXiv:2310.02915 [cond-mat.supr-con]
[31] Liu Y B, Mei J W, Ye F, Chen W Q, and Yang F 2023 *Phys. Rev. Lett.* **131** 236002
[32] Yang Q G, Wang D, and Wang Q H 2023 *Phys. Rev. B* **108** L140505
[33] Zhang Y, Lin L F, Moreo A, Maier T A, and Dagotto E 2023 *Phys. Rev. B* **108** 165141
[34] Sakakibara H, Kitamine N, Ochi M, and Kuroki K 2024 *Phys. Rev. Lett.* **132** 106002
[35] Zhang Y, Lin L F, Moreo A, Maier T A, and Dagotto E 2024 *Nat. Commun.* **15** 2470
[36] Ryee S, Witt N, and Wehling T O 2023 arXiv:2310.17465 [cond-mat.supr-con]
[37] Zhang Y, Lin L F, Moreo A, Maier T A, and Dagotto E 2024 *Phys. Rev. B* **109** 045151
[38] Lange H, Homeier L, Demler E, Schollwöck U, Grusdt F, and Bohrdt A 2024 *Phys. Rev. B* **109** 045127
[39] Yang H, Oh H, and Zhang Y H 2023 arXiv:2309.15095 [cond-mat.str-el]
[40] Oh H and Zhang Y H 2023 *Phys. Rev. B* **108** 174511
[41] Kakoi M, Kaneko T, Sakakibara H, Ochi M, and Kuroki K 2023 arXiv:2312.04304 [cond-mat.supr-con]
[42] Shen Y, Qin M P, and Zhang G M 2023 *Chin. Phys. Lett.* **40** 127401
[43] Jiang R S, Hou J N, Fan Z Y, Lang Z J, and Ku W 2024 *Phys. Rev. Lett.* **132** 126503
[44] Heier G, Park K, and Savrasov S Y 2024 *Phys. Rev. B* **109** 104508
[45] Fan Z, Zhang J F, Zhan B, Lv D S, Jiang X Y, Normand B, and Xiang T 2023 arXiv:2312.17064 [cond-mat.supr-con]
[46] Zhang Y, Lin L F, Moreo A, and Dagotto E 2023 *Phys. Rev. B* **108** L180510
[47] LaBollita H, Pardo V, Norman M R, and Botana A S 2023 arXiv:2309.17279 [cond-mat.str-el]
[48] Chen X J, Jiang P H, Li J, Zhong Z C, and Lu Y 2023 arXiv:2307.07154 [cond-mat.supr-con]
[49] Sui X L, Han X R, Chen X J, Qiao L, Shao X H, and Huang B 2023 arXiv:2312.01271 [cond-mat.mtrl-sci]
[50] Geisler B, Fanfarillo L, Hamlin J J, Stewart G R, Hennig R G, and Hirschfeld P J 2024 arXiv:2401.04258 [cond-mat.supr-con]
[51] Zhang Y, Su D J, Huang Y, Sun H L, Huo M W, Shan Z Y, Ye K X, Yang Z H, Li R, Smidman M, Wang M, Jiao L, and Yuan H Q 2023 arXiv:2307.14819 [cond-mat.supr-con]
[52] Zhou Y Z, Guo J, Cai S, Sun H L, Wang P Y, Zhao J Y, Han J Y, Chen X T, Wu Q, Ding Y, Wang M, Xiang T, Mao H K, and Sun L L 2023 arXiv:2311.12361 [cond-mat.supr-con]
[53] Wang L H, Li Y, Xie S Y, Liu F Y, Sun H L, Huang C X, Gao Y, Nakagawa T, Fu B Y, Dong B, Cao Z H, Yu R Z, Kawaguchi S I, Kadobayashi H, Wang M, Jin C Q, Mao H K, and Liu H Z 2023 arXiv:2311.09186 [cond-mat.supr-con]
[54] Wang H Z, Chen L, Rutherford A, Zhou H D, and Xie W W 2024 *Inorg. Chem.* **63** 5020
[55] Liu Z, Huo M W, Li J, Li Q, Liu Y C, Dai Y M, Zhou X X, Hao J H, Lu Y, Wang M, and Wen H H 2023 arXiv:2307.02950 [cond-mat.supr-con]
[56] Kakoi M, Oi T, Ohshita Y, Yashima M, Kuroki K, Kato T, Takahashi H, Ishiwata S, Adachi Y, Hatada N, Uda T, and Mukuda H 2023 arXiv:2312.11844 [cond-mat.str-el]
[57] Chen K W, Liu X Q, Jiao J C, Zou M Y, Luo Y X, Wu Q, Zhang N Y, Guo Y F, and Shu L 2023 arXiv:2311.15717 [cond-mat.str-el]
[58] Xu M Y, Huyan S Y, Wang H Z, Bud'ko S L, Chen X L, Ke X L, Mitchell J F, Canfield P C, Li J, and Xie W W 2023 arXiv:2312.14251 [cond-mat.supr-con]
[59] Dong Z H, Huo M W, Li J, Li J Y, Li P C, Sun H L, Lu Y, Wang M, Wang Y Y, and Chen Z 2023 arXiv:2312.15727 [cond-mat.supr-con]
[60] Talantsev E F and Chistyakov V V 2024 arXiv:2401.00804 [cond-mat.supr-con]
[61] Castellani C, Natoli C R, and Ranninger J 1978 *Phys. Rev. B* **18** 4945
[62] Zhang F C, Gros C, Rice T M, and Shiba H 1988 *Supercond. Sci. Technol.* **1** 36
[63] Li C H 2009 *Gutzwiller Approximation in Strongly Correlated Electron Systems, Ph.D. Dessertation* (Boston College)
[64] Zhai H, Wang F, and Lee D H 2009 *Phys. Rev. B* **80** 064517
[65] Maier T A and Scalapino D J 2011 *Phys. Rev. B* **84** 180513
[66] Lin L F, Zhang Y, Alvarez G, Moreo A, and Dagotto E 2021 *Phys. Rev. Lett.* **127** 077204
[67] Scalapino D J, White S R, and Zhang S C 1992 *Phys. Rev. Lett.* **68** 2830
[68] Scalapino D J, White S R, and Zhang S C 1993 *Phys. Rev. B* **47** 7995
[69] Hazra T, Verma N, and Randeria M 2019 *Phys. Rev. X* **9** 031049
[70] Sigrist M, Rice T M, and Zhang F C 1994 *Phys. Rev. B* **49** 12058
[71] Ma T X, Wang D, and Wu C J 2022 *Phys. Rev. B* **106** 054510